Available online at www.sciencedirect.com
ScienceDirect
Trans. Nonferrous Met. Soc. China 35(2025) 975−989
Transactions of Nonferrous Metals Society of China
www.tnmsc.cn

Recovery of polymetallic elements from cyanide tailings via reduction smelting

Gong-hao LI, Fen JIAO, Chen LI, Si-yu GU, Shi-yang LIU, Xin WEI

School of Minerals Processing and Bioengineering, Central South University, Changsha 410083, China

Received 18 July 2023; accepted 17 April 2024

Abstract: A process for treating cyanide tailings was proposed. The process essentially implicates reduction smelting which involves volatilizing silver, lead, and zinc in the cyanide tailings at high temperatures. Meanwhile, gold and copper combine with the reduced iron to form a metal phase, allowing for the simultaneous recovery of polymetallic elements. The experimental results indicate that the process works optimally with a coke powder of 7.5 wt.%, an alkalinity of 1.0, a melting temperature of 1450 °C, and a melting time of 60 min. Under these conditions, more than 99% of gold, 77% of copper and 94% of iron are incorporated into pig iron. In the meantime, the volatilization rate of silver exceeds 90%, while lead and zinc are essentially completely volatilized. The primary component of the by-product smelting slag is akermanite, which exhibits lower leaching toxicity than the national standard and belongs to general solid waste. Additionally, taking the trapping process of iron to copper as a case study, the mechanism of iron trapping is methodically examined and divided into three processes: smelting reduction, migration capture, and condensation deposition.

Key words: cyanide tailings; gold tailings; reduction smelting; valuable element recovery

1 Introduction

Cyanidation is currently the most extensively used approach of gold extraction worldwide, with more than 85% of gold extracted through this technique [1]. A large amount of cyanide tailings can be produced during cyanide leaching. According to statistics, cyanide tailings reserves in China can reach 1×10^8 t [2]. Cyanide tailings are hazardous solid wastes produced during cyanide leaching. They exhibit strong toxicity [3], pose significant threats to surrounding environment [4], and present serious safety risks [5]. In the meantime, cyanide tailings contain gold, silver, copper, iron, and other valuable elements [6,7]. If they undergo secondary resource recovery, safety issues and resource wastage are reduced. Overall, the development of efficient, clean, and high-value utilization technologies for cyanide tailings will be a key direction of future research given the large reserves, serious contamination, and complex characteristics of cyanide tailings.

The utilization technologies for cyanide tailings include the use of construction materials [8−10], advanced leaching [11−13], magnetic roasting from magnetic separation [14,15], and chlorination roasting [16,17]. For these approaches, the use of cyanide tailings as a raw material for building materials leads to the waste of valuable elements. Continuous leaching retains more leaching slag and cannot achieve tailings reduction [14]. Magnetic roasting–magnetic separation is mostly utilized to recover iron, but it is difficult to recover other elements [18]. Chlorination roasting is able to realize the separation and recovery of valuable

Corresponding author: Fen JIAO, Tel: +86-13549683403, E-mail: jfen0601@126.com
DOI: https://doi.org/10.1016/S1003-6326(24)66728-2

elements, but it produces pollution; therefore, it currently does not conform to the concept of environmental protection [19].

As a metallurgical process, reduction smelting technology is able to reduce the cost of treating low-grade secondary resources, including cyanide tailings, steel mill dust, and anode mud [20]. If the cyanide tailings are reduced through high-temperature carbothermal reduction, the valuable elements in the cyanide tailings will eventually be converted to metallic elements in the high-temperature and reducing atmosphere. Currently, volatile elements, such as silver, lead, and zinc, can be separated through volatilization, while non-volatile elements such as gold, copper, and iron, remain in the melt. At the same time, it has been reported that the molten metals dissolve other metals with varying solubility [21]. For instance, copper and lead are commonly utilized as collectors of precious metals in fire assays [22]. TIAN et al [23] recovered nickel from nickel-based superalloy using molten zinc, and the recovery efficiency reached 95.2%. DING et al [24] recovered platinum group metals from scrap automobile catalysts through iron smelting and achieved a recovery efficiency of 99% in their pilot experiment. Supercritical extraction of residual oil, which uses copper as a collector of platinum group metals, has been adopted by Japanese Companies [25]. PENG et al [26] developed a process that employs iron as a collector. DONG et al [27] also utilized molten metals to recover platinum group metals, gold, silver, and rare metals. The obtained results revealed the potential of using molten metals as metal collectors. For example, gold and copper can be extracted from iron, and valuable elements can be fully recovered from cyanide tailings. Compared with other techniques, this approach exhibits many advantages, including low contamination, simple and flexible operation, and wide applicability.

In the present investigation, a new process for treating cyanide tailings was proposed. The reduced smelting was able to effectively eliminate the pollution caused by cyanide, promote the volatilization of silver, lead, and zinc at high temperatures, and employ the reduced liquid iron to capture gold and copper. Finally, the separation of ferrosilicon was achieved through the separation of metal and slag phases, and the recovery of many valuable elements was achieved, providing a new treatment idea for other solid wastes.

The volatilization of silver, lead, and zinc under smelting conditions was confirmed. The migration law of gold and copper during smelting and the factors affecting this process were systematically studied. The feasibility of using iron as a scavenger was confirmed, the smelting slag was characterized, and a novel and harmless method to recover valuable elements in cyanide tailings was provided.

2 Experimental

2.1 Materials

The experimental raw materials used in this work were obtained from roasting−cyanidation tailings produced by roasting−cyanidation leaching of a smelter in Henan Province, China. Table 1 presents the major chemical composition of the dried raw materials, whereas Fig. 1 shows the X-ray diffraction (XRD) pattern of the experimental raw materials.

Table 1 Chemical composition of cyanide tailings (wt.%)

Au*	Ag*	Cu	Fe	Si	Al
1.09	46.66	0.24	32.72	19.58	3.40
Ca	Pb	Zn	S	As	CN*
1.67	1.01	0.93	1.77	0.14	18.40

* g/t

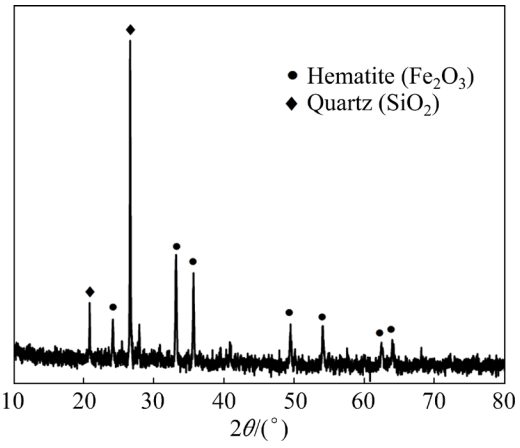

Fig. 1 XRD pattern of cyanide tailings

Table 1 indicates that the main elements in the cyanide tailings are iron and silicon, with contents of 32.72 wt.% and 19.58 wt.%, respectively. The contents of gold and silver are 1.09 and 46.66 g/t, respectively. The contents of copper, lead and Zn

are 0.24 wt.%, 1.01 wt.%, 0.93 wt.%, respectively. Small amounts of calcium, aluminum, and other elements are also found. The contents of sulfur, arsenic, and cyanide were determined as 1.77 wt.%, 0.14 wt.%, and 18.40 g/t, respectively. Figure 1 illustrates that the primary minerals in the slag are hematite and quartz. Other minerals may not exhibit an obvious diffraction peak in the XRD pattern due to their low contents.

The reagents used in the experiment were all purchased from Sinopharm Chemical Reagent Co., Ltd. The properties of the coke powder used are presented in Table 2.

Table 2 Composition of coke powder (wt.%)

Fixed carbon	Ash	Volatile component
91.59	5.88	2.53

2.2 Experimental procedures

The cyanide tailings, slagging agent, and reducing agent were mixed equally following a specific ratio and then placed in a corundum crucible. The smelting test was performed in an induction furnace (SP−85KTC, Kejing, China). The products were taken out at the end of smelting. The slag and metal phases were manually separated, weighed, and sampled for the analysis.

2.3 Characterization method and evaluation index

The iron smelting slag type was $CaO-SiO_2-MgO-Al_2O_3$, and the mass ratio of each oxide was controlled to be $m(CaO):m(SiO_2):m(MgO):m(Al_2O_3)=4:4:1:1$ during batching. The definition of alkalinity (R) is presented by Eq. (1):

$$R=(m_{MgO}+m_{CaO})/(m_{Al_2O_3}+m_{SiO_2}) \quad (1)$$

where m_{MgO}, m_{CaO}, $m_{Al_2O_3}$, and m_{SiO_2} are the masses of MgO, CaO, Al_2O_3, and SiO_2, respectively.

The gold and silver assays were determined by fire assay (conducted at Changsha Institute of Mining and Metallurgy, China). Iron was titrated with potassium dichromate and the quantitative analyses of Cu, Pb, and Zn were performed by inductively coupled plasma emission spectroscopy (FMX26, SPECTROBLUE, Germany) after completely dissolving with aqua regia.

The ratio of the content of a valuable element in pig iron to the total amount of that element is defined as the recovery efficiency of that element, which can be calculated in the following form:

$$\varepsilon=(m_1\cdot\omega_1)/(m_0\cdot\omega_0)\times100\% \quad (2)$$

where ε represents the recovery efficiency, m_1 and ω_1 in order denote the mass of the metal phase (g) and the element content of the metal phase (wt.% or g/t), m_0 and ω_0 stand for the mass of the raw material (g) and the element content of the raw material (wt.% or g/t), respectively.

The volatilization loss of elements is defined as the volatilization rate, which is evaluated as follows:

$$\gamma=[1-(m_1\cdot\omega_1)/(m_0\cdot\omega_0)-(m_2\cdot\omega_2)/(m_0\cdot\omega_0)]\times100\% \quad (3)$$

where γ is the volatilization rate, m_2 and ω_2 in order signify the mass of the slag phase (g) and the element content of the slag phase (wt.% or g/t).

2.4 Theoretical fundamental

Reduction smelting involves high temperatures and a strong reducing atmosphere, and therefore, it can be expected that the main valuable metal elements in the cyanide tailings after the reduction smelting treatment will eventually exist in elemental form. The conventional temperature of iron making usually exceeds 1400 °C. Figure 2 [28] illustrates that when the temperature exceeds 1400 °C, silver, lead, and zinc have higher saturation vapor pressure and leave the melt through volatilization. Meanwhile, gold, iron, and copper have lower saturation vapor pressures and remain in the melt at high temperatures.

The high-temperature melt consists of two parts: metal melt and liquid slag. The major component of the slag phase is silica aluminate, a configuration that is mainly dominated by local electrons. Gold, copper, and iron belong to metals,

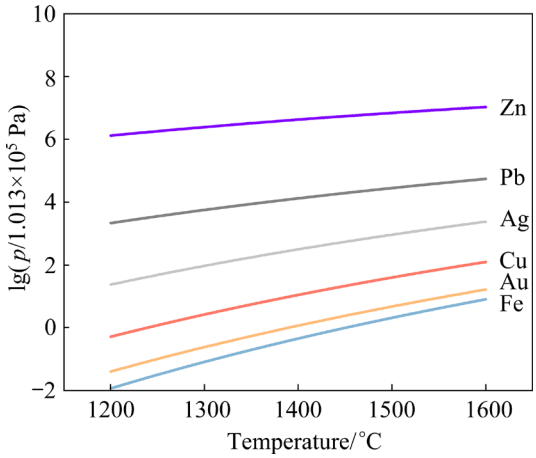

Fig. 2 Relationship between saturation vapor pressure and metal temperature [28]

thus their electron cloud configurations are dominated by non-local electrons. The two types of electron clouds do not interact with each other, and therefore, gold and copper tend to bond with iron [29]. In addition, iron is converted to γ-Fe at high temperatures, where γ-Fe possesses the same structure and lattice parameters as those of gold and copper. According to the Hume−Rothery rule, solid solutions may be composed of gold, copper, and iron [30]. Further, gold and copper exhibit high electronegativity and positive standard electrode potential. These metals or their oxides are the first to be reduced during smelting. By the time the iron oxide is completely converted to iron, gold and copper have already converted to atomic states or clusters, facilitating their binding to iron [31]. The gold–iron (Fig. 3(a)) and copper−iron (Fig. 3(b)) phase diagrams obtained using Factsage 8.0 also reveal that gold and copper are able to combine with iron to form alloys at high temperatures. Figure 3(c) illustrates that the enriched γ-Fe phase of copper and gold exhibits a carburization reaction during smelting, lowers the melting point of the alloy, promotes the melting of the alloy, makes the alloy appear liquid, gathers at the bottom of the crucible under the action of gravity and realizes the separation of the gold and slag phase.

3 Results and discussion

3.1 Effects of reaction conditions on recovery of gold, copper, and iron

3.1.1 Influence of reductant

Figure 4 illustrates the influence of reducing agent dose on the iron reduction and the capture. The recovery efficiency of gold and iron initially increases and then decreases with increasing the coke dosage during smelting. When the coke dosage reaches 7.5 wt.%, the highest gold and iron recovery efficiency values are 99.76% and 94.04%, respectively. As the reducing agent dosage reaches 12.5 wt.%, the recovery efficiency values of gold and iron show a decrease of 22.84% and 4.23%, respectively, whilst when the coke powder content exceeds 10 wt.%, the recovery efficiency of copper basically remains stable.

The variation plot of the carbon content of the non-metallic phase is presented in Fig. 5. A rapid decrease of the carbon content in the non-metallic phase is evident at 15 min before melting. This

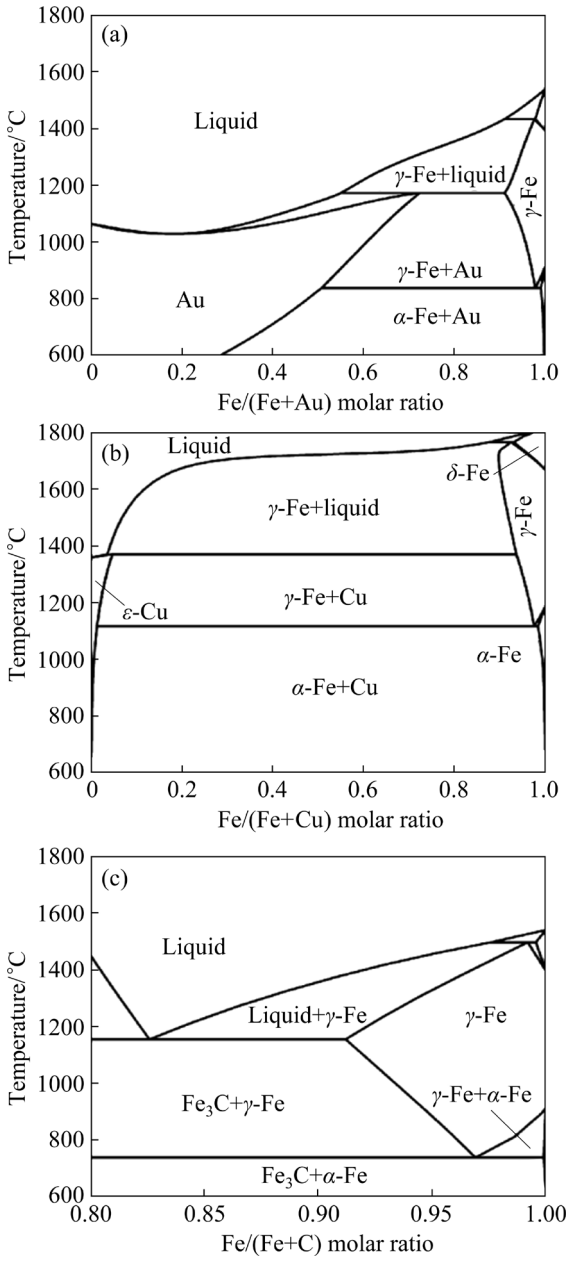

Fig. 3 Phase diagrams of gold–iron (a), copper–iron (b), and carbon–iron (c)

phenomenon is primarily attributed to the initial formation of the metallic phase. In cases where the dosages of coke powder are 2.5 wt.% and 5 wt.%, respectively, the amount of reducing agent is not enough and the reducing atmosphere during smelting is weak. Fe_2O_3 is not completely converted to iron and there is more iron in the form of FeO in the slag [32]. On the contrary, when the dosage of coke powder reaches 10 wt.% and 12.5 wt.%, respectively, more than 2 wt.% carbon remains in the non-metallic phase. This part of carbon leads to the increase in slag viscosity, deterioration of the

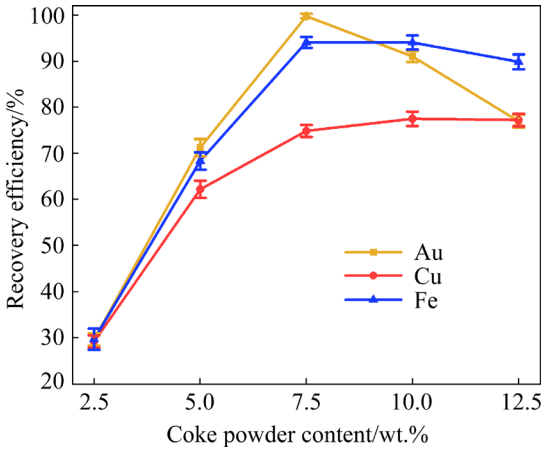

Fig. 4 Effect of coke powder content on recovery efficiencies of gold, copper, and iron

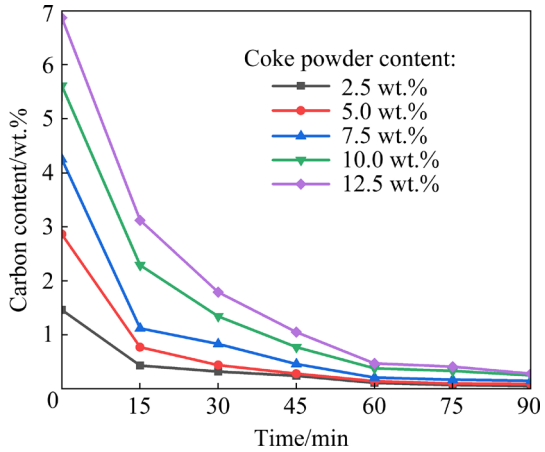

Fig. 5 Variation of carbon content in non-metallic phase

fluidity of the slag phase, difficulty in gathering liquid iron, and the decrease in grade and recovery of iron [33].

The capture process of gold by iron can be regarded as the process of combining gold with iron through the slag phase. In the completely molten state, its diffusion coefficient (D) meets the requirements of the Einstein−Stokes equation:

$$D=k_{\mathrm{B}}T/(6\pi\eta r) \quad (4)$$

where k_{B} represents the Boltzmann constant, T denotes the thermodynamic temperature, η is the dynamic viscosity of the solution, and r signifies the atomic radius of the solute.

Viscosity has a significant effect on gold diffusion in the slag phase. Generally, the higher the viscosity of the slag phase is, the more difficult for gold to diffuse and come into contact with iron and collect iron. Furthermore, the limited gold content prevents the formation of particles large enough to sink, such as copper and iron, which limits gold recovery potential.

The experiment proves that the amount of reducing agent is one of the crucial factors that affect the recovery of gold, copper, and iron. It also validates the feasibility and reliability of the smelting reduction method.

3.1.2 Influence of alkalinity

The alkalinity of smelting slag plays a pivotal role in determining its properties. The influence of alkalinity on metal recovery is illustrated in Fig. 6.

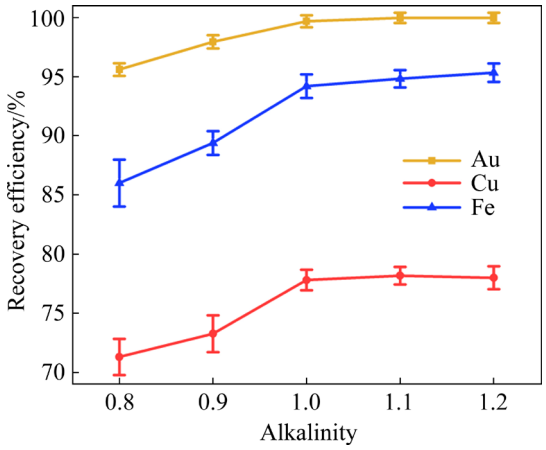

Fig. 6 Effect of alkalinity on recovery efficiencies of gold, copper, and iron

The obtained results reveal that with higher alkalinity, the recovery efficiency of gold, copper, and iron at basicity 1.0 reaches 99.70, 77.81%, and 94.50%, respectively; thereafter, they tend to remain stable. Alkalinity plays a crucial role in smelting. It directly affects the viscosity of the smelting slag and indirectly affects the metal recycling efficiency.

Figure 7 demonstrates the change in the viscosity of the smelting slag liquid at various alkalinities. Obviously, the viscosity of the slag phase decreases with increasing the alkalinity. The main component of the slag phase is silicate. According to the polymer theory, silicate melt in a completely molten state is composed of cations and complex Si−O anion groups. The Si−O anion groups are connected by the silicon−oxygen tetrahedron $[SiO_4]^{4-}$ through the bridging oxygen [34,35] and O^{2-} is produced simultaneously, as displayed by Eqs. (5) and (6):

$$2[SiO_4]^{4-}=[Si_2O_7]^{6-}+O^{2-} \quad (5)$$

$$3[SiO_4]^{4-}=[Si_3O_{10}]^{8-}+2O^{2-} \quad (6)$$

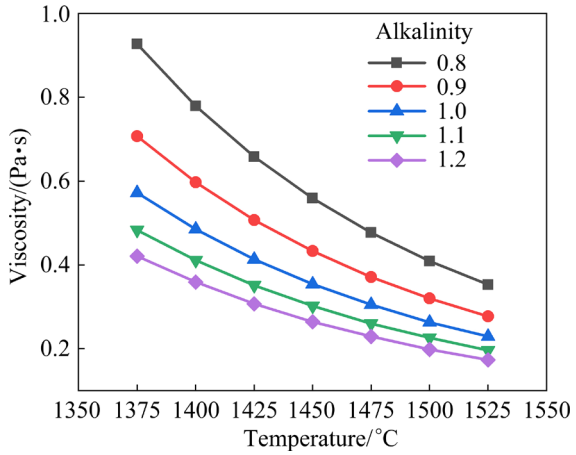

Fig. 7 Effect of alkalinity on viscosity of smelting slag liquid

The main cations of the slag phase are Ca^{2+} and Mg^{2+}, which belong to variable network ions and exhibit the characteristics of small charge, large radius, and high metal activity. The ability to compete for O^{2-} is weak. In the melt, the cations are hexagonal or exhibit higher coordination with non-bridging or free oxygen located between the silico−oxygen tetrahedron $[SiO_4]^{4-}$, which could weaken the melt polymerization [36]. An increase in basicity indicates an increase in Ca^{2+} and Mg^{2+} contents, which causes the differentiation of the complex Si−O anion groups into smaller units, and thus reduces the viscosity of the slag phase, increases its fluidity, reduces the inclusion of ferroalloys, and improves recovery efficiency of metals.

In addition, some iron will be present in the form of fayalite due to the high content of SiO_2 in the test raw materials. This condition prevents recovery efficiency of iron [37].

$$2FeO+SiO_2=Fe_2SiO_4 \quad (7)$$

Under reducing conditions, fayalite reacts with the added CaO and MgO to produce metallic iron and olivine [38,39]:

$$2CaO+Fe_2SiO_4+2C=Ca_2SiO_4+2CO+2Fe \quad (8)$$

$$2MgO+Fe_2SiO_4+2C=Mg_2SiO_4+2CO+2Fe \quad (9)$$

Therefore, higher alkalinity is beneficial to iron recovery and trapping. Simultaneously, SINEVA et al [40] argued that CaO and MgO indirectly affect the copper capacity of slag by affecting the iron/silicon ratio. In addition, increasing the contents of CaO and MgO helps to reduce the solubility of copper in the slag and increase the entry of copper into the metal phase. It should be noted that the investigations by SHISHIN et al [41] also support the above views.

3.1.3 Influence of smelting temperature

To obtain the effect of smelting temperature on metal recovery efficiency, the change of metal recovery efficiency during smelting process at temperatures from 1400 to 1500 °C is investigated. Figure 8 illustrates the recovery efficiency of the metals as a function of smelting temperature.

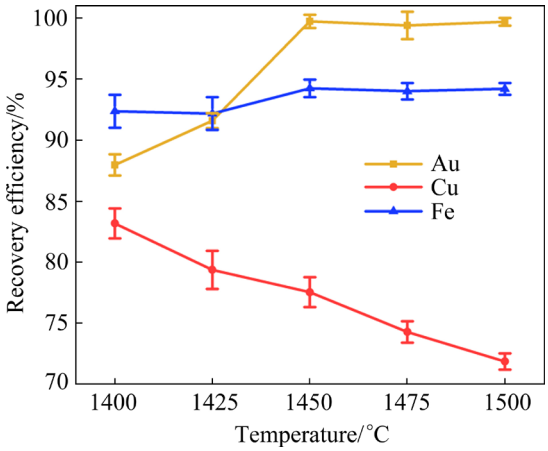

Fig. 8 Effect of smelting temperature on recovery efficiencies of gold, copper and iron

The experimental results indicate that the recovery efficiency of gold grows from 87.95% to more than 98.00% and remains at a relatively stable level with increasing temperature from 1400 to 1500 °C, meanwhile the recovery efficiency of iron enhances from 92.35% to 94.23%. However, the copper recovery efficiency decreases significantly from 83.16% (1400 °C) to 71.84% (1500 °C).

In general, an increase in smelting temperature leads to an increase in the excessive energy for smelting, making dissociating into small silicon−oxygen tetrahedra easier for the complex Si−O anion groups of large molecules in the slag (Eq. (10)):

$$[Si_2O_6]_n^{4n-}+2n[O]=2nSiO_4^{2-} \quad (10)$$

The results presented in Fig. 7 also prove that the slag viscosity lessens with increasing temperature and slag fluidity increases. These conditions are more favorable for the capture and settlement of iron particles, and the recovery efficiencies of iron and gold increase at the same time. However, some iron remains in the slag as

iron olivine due to high silicon content, resulting in iron loss.

YANNOPOULOS [42] pointed out that increasing the temperature will enhance the solubility of copper and sulfur in the slag, resulting in a metal loss. HIDAYAT et al [43] demonstrated that in the Fe−Cu−O−Si system, increasing the copper activity in the Fe−Cu alloy leads to an increase in the solubility of copper in the slag and, as a result, an increase in copper loss.

An increase in temperature leads to the growth of the vapor pressure of the liquid metal, increases copper activity, and then decreases copper recovery efficiency. The experimental data and simulation results also prove that copper recovery efficiency is negatively correlated with temperature. The experimental results reveal that the temperature has a significant effect on the metal recovery, and the optimal smelting temperature will be 1450 °C.

3.1.4 Influence of smelting time

Figure 9 illustrates the change of metal recovery efficiency with smelting time. The recovery efficiency of gold and iron increases to 98.97% and 94.41%, respectively, after 60 min of smelting and remains stable. The copper recovery efficiency decreases from the initial value of 80.56% to 77.4% and then to 75.89% at 90 min.

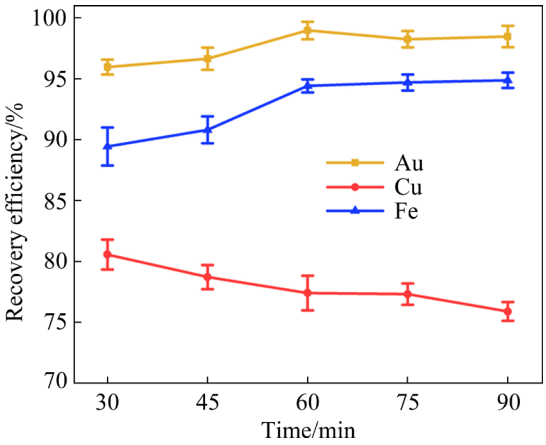

Fig. 9 Effect of smelting time on recovery efficiencies of gold, copper, and iron

The smelting time indirectly affects the metal recovery by affecting the composition of the smelting atmosphere. In the special case of a smelting time of 30 min, the reducing agent remains unreacted in the slag phase, and the smelting atmosphere represents a strong reducibility. These conditions are favorable to the presence of copper in elemental form. At this point, only about 90% of iron is reduced. Reducing the amount of iron and shortening the smelting time also weaken the effect of iron on gold collection and thus reduces gold recovery.

After smelting for 60 min, more reducing agent in the slag is consumed, the reducing atmosphere weakens, the solubility of copper in the slag increases, and the reduced copper returns to the slag, thus reducing the recovery efficiency of copper [44]. Increasing the smelting time is more beneficial to iron reduction and precipitation, and simultaneously prolongs the collection time and increases the recovery efficiency of iron and gold.

When the smelting time reaches 90 min, the reducing agent is almost completely consumed, the oxygen potential continues to increase, and the solubility of copper in the slag increases simultaneously, leading to further reduction of copper recovery efficiency. The higher oxygen potential also causes iron to enter the slag [45]. However, the iron recovery loss is lower due to the higher iron content of the materials used in the experiment. Compared to copper and iron, oxygen potential has less effect on gold recovery [46]. As the smelting time increases, the iron and gold recovery efficiencies become more stable.

The obtained results reveal that smelting time has a special effect on the metal recovery. In addition, the best smelting time is obtained as 60 min.

3.1.5 Properties of products

In summary, the optimal conditions (reducing agent dosage 7.5 wt.%, alkalinity 1.0, smelting temperature 1450 °C, and smelting time 60 min) can be chosen to obtain the appropriate metal products. The contents of iron, copper, and gold in pig iron and smelting slag are presented in Table 3. A comparison between the raw ore and the slag phase reveals a substantial lessening in the content of each element, indicating the effective separation of metallic elements from the slag phase and their

Table 3 Contents of iron, copper, and gold in pig iron and smelting slag (wt.%)

Sample	Fe	Cu	Au*
Pig iron	92.85	0.56	3.32
Smelting slag	0.82	0.036	–

* g/t

enrichment in pig iron. The obtained results reveal the potential of iron as a gold and copper trapping agent and highlight the promising application prospects of this method.

3.1.6 Recovery mechanism

To clarify the trapping of valuable elements by iron and to understand the law of migration of elements, this study presents the trapping of iron on copper as an example, and CuO to increase the copper content of raw ore up to 8 wt.% to examine the trapping of iron under the conditions of 7.5 wt.% reducing agent, alkalinity 1.0, and smelting temperature 1450 °C. The variations of mixed materials during reduction smelting are illustrated in Fig. 10.

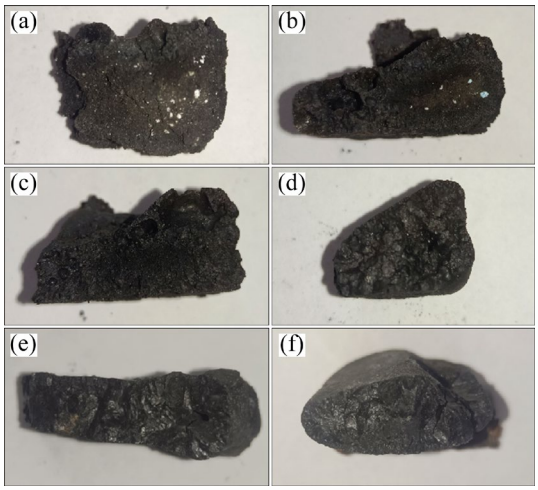

Fig. 10 Changes in mixed materials during reduction smelting for various time: (a) 2 min; (b) 5 min; (c) 7 min; (d) 10 min; (e) 20 min; (f) 30 min

For the case of the smelting time of 2 min, Fig. 10(a) clearly demonstrates that the mixed material is loose and has distinct particles, indicating that the reaction at this time is dominated by the solid phase reaction. As smelting continues for 5 min (Fig. 10(b)), the mixture melts from the outside to the inside, producing a liquid phase with only a small region in the middle remaining unmelted. When the smelting time is increased to 7 min (Fig. 10(c)), the solid-phase reaction zone continues to shrink, whereas the liquid-phase reaction zone expands. At this point, the mixture is essentially completely melted, except for some interior regions. Finally, at 10 min (Fig. 10(d)), the solid-phase reaction zone completely disappears and the slag phase is initially formed and separated from the metal phase. At smelting time of 20 and 30 min, the appearance of the slag phase is similar to that of 10 min, without considerable change. Therefore, we can divide the mixture behavior during the smelting process into three processes: solid-phase reaction, liquid-phase reaction, and slag–metal separation process.

Scanning electron microscopy (SEM) energy dispersive X-ray spectroscopy (EDS) analysis was performed for three processes. As illustrated in Fig. 11(a), many particles of different sizes still exist in the solid-phase reaction, indicating that the mixed materials remain dispersed at this stage and have not contacted and reacted. The white binary alloys formed by reduced iron and copper can be seen in Fig. 11(b), and these alloys exhibit an initial separation from the grey slag phase. The point scan results show that the contents of iron and copper in the slag phase are less than 3%, which indicates that most of the iron and copper are reduced to an elemental state. The distribution of the elements indicates that the iron forms many distinct bright spots, proving that it forms a slight agglomeration, but the copper is still uniformly dispersed in the mixture, and no definite zone of agglomeration is detected. Therefore, the key reaction in the solid-phase reaction stage mainly incorporates the reduction of metal oxides.

Figure 12 illustrates the morphology of the liquid-phase reaction zone. No granular material is detectable in Fig. 12(a), and a large white alloy zone with a distinct boundary in the grey slag phase zone is visible at lower magnification. Compared to Fig. 11(a), the alloy region in Fig. 12(a) is significantly larger, and the small and medium-sized metal droplets aggregate and grow into larger metal particles during this migration process. The point scan results of Fig. 12(b) demonstrate that the contents of iron and copper elements in the slag phase are less than 1.5%, which exhibits a relatively obvious reduction. In addition, the distribution of iron and copper elements in Figs. 12(c−e) is relatively concentrated, and there is an obvious overlap, indicating that individual metals are captured during the migration, aggregation, and growth of metal droplets. That is, free metals are recovered in the liquid-phase reaction stage.

Figures 13 and 14 demonstrate the images of the slag phase and metallic phase, respectively. In Fig. 13, only a grey slag phase can be seen, which

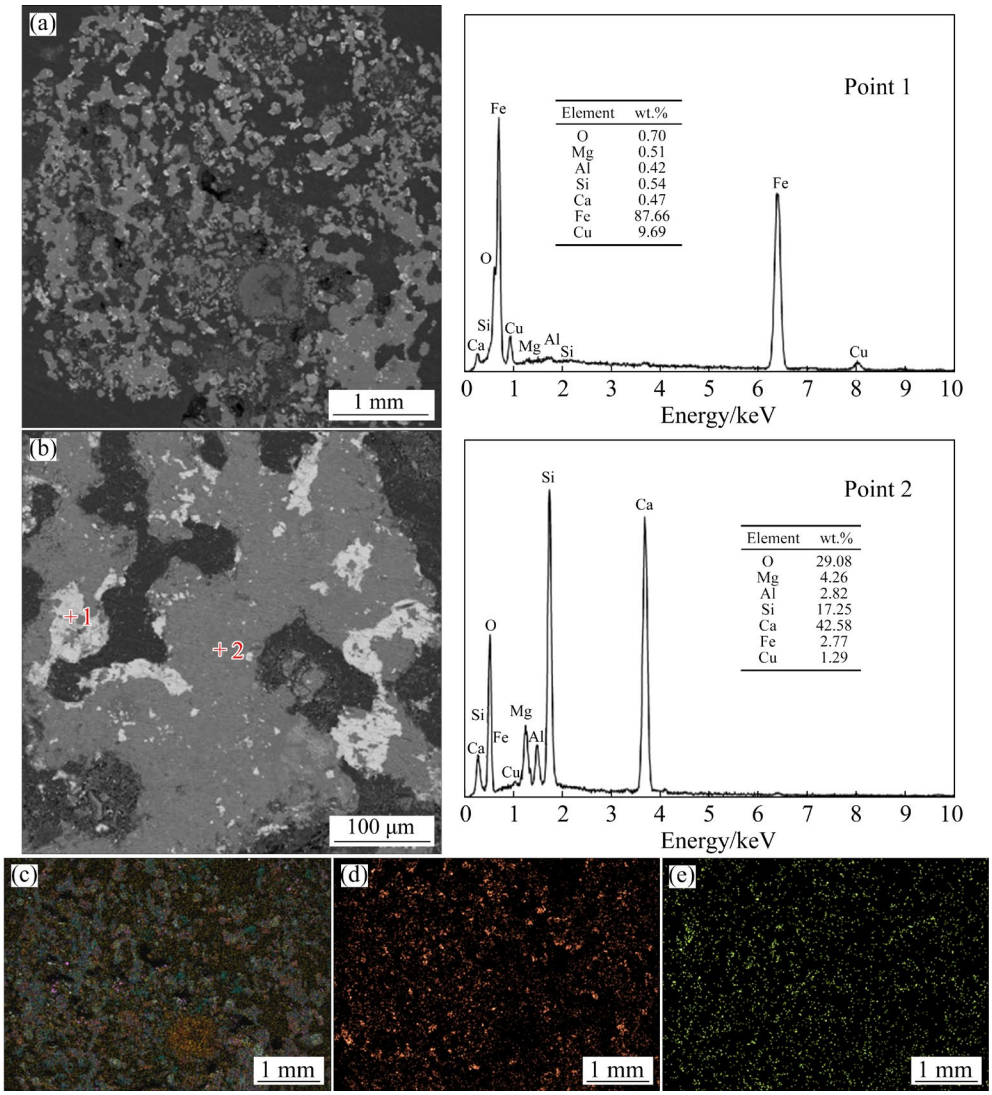

Fig. 11 SEM−EDS analysis results of solid-phase reaction zone: (a) Lower magnification SEM image; (b) Higher magnification SEM image; (c) Full elemental distribution; (d) Distribution of iron; (e) Distribution of copper

shows that the slag phase is completely separated from the metal phase. The surface scanning results (Figs. 13(c−e)) reveal that a certain amount of iron and copper is uniformly distributed in the slag phase, and some iron and copper are lost in this phase. The specific causes of loss should be further analyzed.

As illustrated in Fig. 14, only a single region can be observed in the resulting alloy, which proves that this alloy is homogeneous in composition and exhibits high purity. The formation of a copper−iron alloy is also confirmed by the presented results in Fig. 14, revealing that iron and copper are uniformly distributed in the metallic phase, and no independent monometallic phase is detectable. In slag–metal separation, the metal particles are condensed into large metal pieces that settle under the effect of gravity to separate from the slag phase.

Based on the above experiments, iron trapping can be rationally divided into three stages: smelting reduction, migration capture, and condensation deposition. Figure 15 schematically demonstrates these processes well.

At the beginning of smelting, metal oxides are converted into metal droplets by reducing agents, which are evenly distributed in the initial stage of slag. As smelting progresses, metal particles aggregate and grow under surface tension to form larger metal particles, during which the entrapment of valuable elements is realized [47]. For this process, ZHENG et al [48] pointed out that the initial concentration of valuable elements in the melt

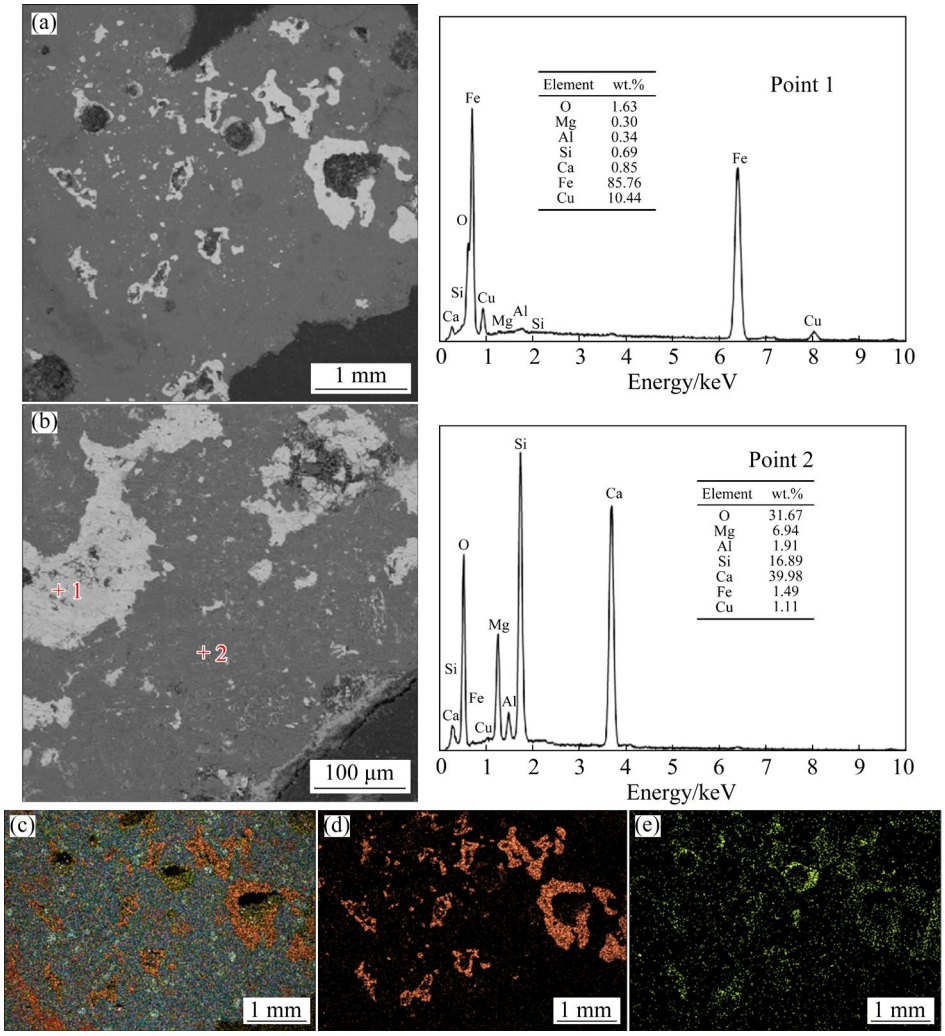

Fig. 12 SEM−EDS analysis results of liquid-phase reaction zone: (a) Lower magnification SEM image; (b) Higher magnification SEM image; (c) Full elemental distribution; (d) Distribution of iron; (e) Distribution of copper

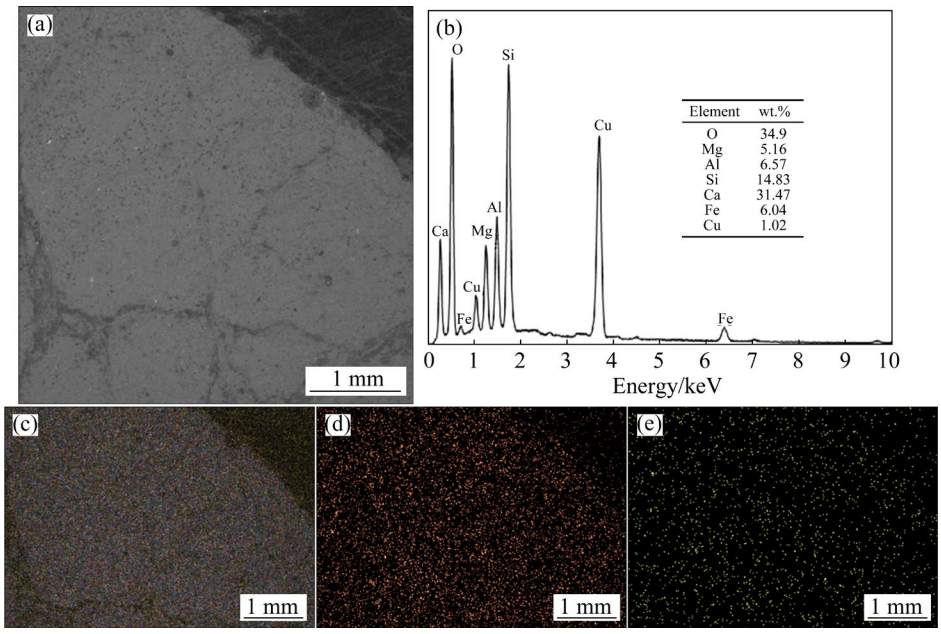

Fig. 13 SEM−EDS analysis results of slag plase: (a) Lower magnification SEM image; (b) EDS data; (c) Full elemental distribution; (d) Distribution of iron; (e) Distribution of copper

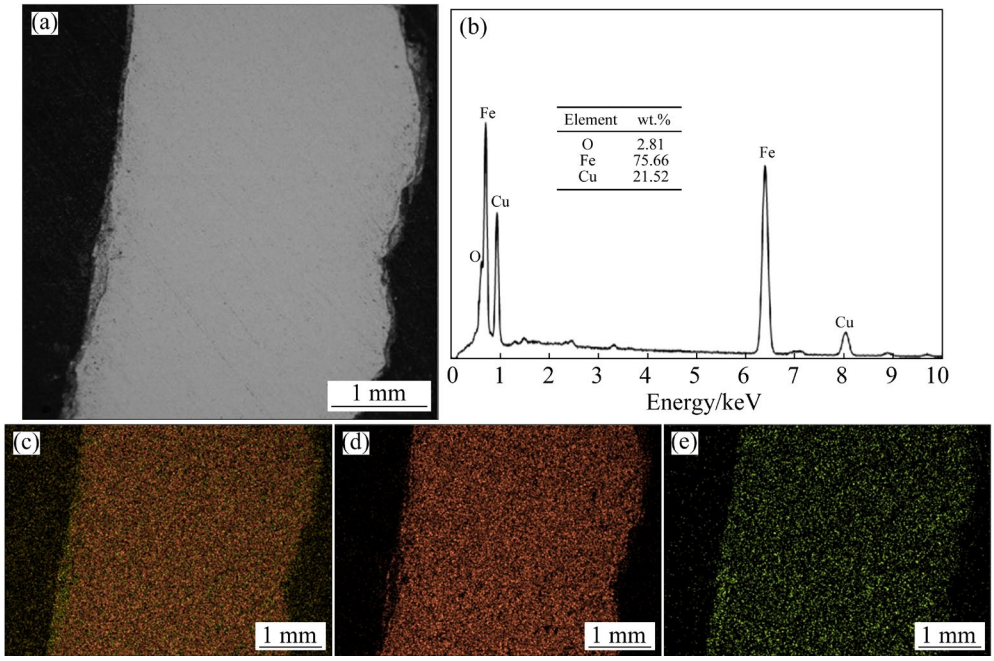

Fig. 14 SEM−EDS analysis results of metallic phase: (a) Lower magnification SEM image; (b) EDS data; (c) Full elemental distribution; (d) Distribution of iron; (e) Distribution of copper

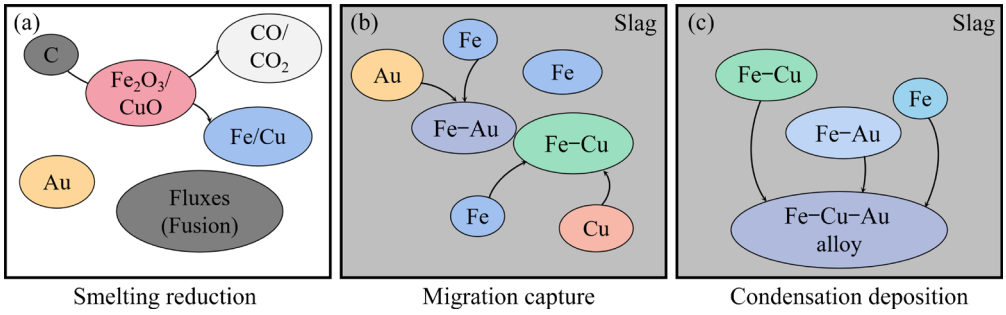

Fig. 15 Iron-trapping mechanism of gold and copper

is very low, and the formation of the droplet precipitation by accumulating to a critical size is difficult and requires the precipitation of iron particles. In the next stage of smelting, the metal particles settle down under the action of gravity force and configure a uniform and single metal phase that is separated from the slag phase. After phase separation, the exchange of matter and energy still occurs between the metal phase and the slag phase. However, the specific bonding process between metals needs to be further investigated.

3.2 Volatilization behavior of metals

The changes in volatilization of various metal elements when melting temperature changed from 1400 to 1500 °C were also methodically scrutinized. The corresponding experimental results are shown in Table 4.

Table 4 Relationship between metal volatilization rate and temperature

Temperature/°C	Volatilization rate/%					
	Au	Cu	Fe	Ag	Pb	Zn
1400	<0.5	<0.5	<0.5	84.37	>99.5	>99.5
1425	<0.5	0.78	<0.5	89.05	>99.5	>99.5
1450	<0.5	1.25	<0.5	91.76	>99.5	>99.5
1475	<0.5	1.88	0.56	94.32	>99.5	>99.5
1500	<0.5	2.37	0.83	95.03	>99.5	>99.5

The obtained results indicate that even when the smelting temperature reaches 1500 °C, the volatilization loss of gold, copper, and iron is less than 2.5%, and most of the loss remains in the melting system. Lead and zinc are highly volatile and can be completely volatilized at 1400 °C. The

volatilization rate of silver reaches 84.37% at 1400 °C and gradually grows with increasing temperature. Therefore, most of the silver will volatilize out of the melt during smelting and can be recovered with lead and zinc. The above experimental results confirm the theoretical basis and reveal that essentially no loss is caused by the volatilization of gold, iron, and copper during the smelting process, while silver, lead, and zinc will leave the melt and can be collected later through condensation.

3.3 Properties of smelting slag

The smelting slag produced under optimal conditions was appropriately analyzed by XRD and the results are presented in Fig. 16. As is seen, SiO_2, CaO, and other materials were not found in the XRD pattern, indicating that the cyanide tailings completely reacted with the slag-making agent and produced a relatively high-quality slag phase. The major component of smelting slag is akermanite, which can be utilized in the production of ceramic glass, cement-based composites, and other building materials.

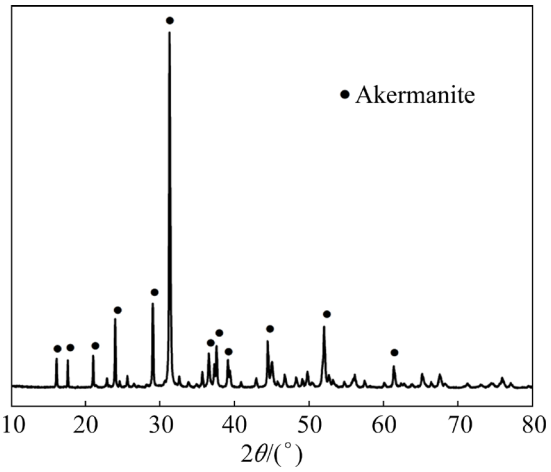

Fig. 16 XRD pattern of slag phase

To investigate the leaching toxicity of the smelting slag, the leaching characteristics of lead, zinc, copper, arsenic, and silver in the smelting slag were examined according to the requirements of HJ/T299—2007. The results were compared with the limit values of the Chinese Standard GB5085.3 — 2007. The leaching results are presented in Table 5. Obviously, the presence of lead, zinc, and silver in the leaching solution could not be detected, and the contents of arsenic and copper were lower than those recommended by the National Standard. The experimental results reveal that the leaching results of lead, zinc, copper, arsenic, silver, and other harmful elements are all lower than the standard values and the smelting slag obtained can be considered as harmless or clean slags. Accordingly, the harmless treatment of cyanide tailings has been successfully achieved.

Table 5 Results of toxic leaching experiment

Element	National standard/ ($mg \cdot L^{-1}$)	Leaching concentration/($mg \cdot L^{-1}$)
Cu	100	0.64
Pb	5	–
Zn	100	–
As	5	0.51
Ag	5	–

4 Conclusions

(1) An effective approach was proposed to recover gold, copper, and iron from cyanide tailings. Through direct reduction smelting, more than 99% of gold, 77% of copper, and 94% of iron were recovered from cyanide tailings under the following conditions: coke dosage of 7.5 wt.%, basicity of 1.0, smelting temperature of 1450 °C, and smelting time of 60 min.

(2) Cyanide tailings are appropriately treated via one-step reduction smelting, and all kinds of metal elements are enriched by the iron-making process. This approach is able to exhibit the simple and mature characteristics, with extensive applicability and simultaneous recovery of various metals.

(3) Only the slag-making and reducing agents are required to be added during the treatment. Additionally, toxic and harmful substances are not produced and the pertinent environmental pollution is relatively low.

(4) By employing the proposed effective approach, toxic cyanide tailings are appropriately converted into non-toxic smelting slag through smelting treatment. Further, the harmless treatment of hazardous solid wastes is appropriately realized.

(5) This investigation provides a novel method for the clean and efficient exploitation of cyanide tailings and a new feasible strategy for the recovery of metallic elements.

CRediT authorship contribution statement

Gong-hao LI: Conceptualisation, Methodology, Literature research, Conducting experiments, Writing − Original draft; **Fen JIAO:** Methodology, Resources, Supervision, Writing − Review and editing, Project administration, Funding acquisition; **Chen LI:** Conducting experiments; Formal analysis; **Si-yu GU:** Investigation, Visualisation; **Shi-yang LIU:** Methodology, Conceptualisation; **Xin WEI:** Software, Investigation.

Declaration of competing interest

The authors declare that they have no known competing financial interests or personal relationships that could have appeared to influence the work reported in this paper.

Acknowledgments

This work is supported by the National Key R&D Program of China (No. 2020YFC1909203) and the Hunan Provincial Innovation Project, China (No. CX20230213).

References

[1] YANG Wei, DONG Hua, CAO Huan, LONG Tao, DENG Sha, WAN He. Lead oxide enhances the leaching of gold in cyanide tailings [J]. JOM, 2023, 75(2): 301−309.

[2] DONG Kai-wei, XIE Feng, WANG Wei, CHANG Yong-feng, LU Dian-kun, GU Xian-wei, CHEN Chun-lin. The detoxification and utilization of cyanide tailings: A critical review [J]. Journal of Cleaner Production, 2021, 302: 126946.

[3] SIERRA-ALVARADO E G, VALLE-CERVANTES S, LUCHO-CHIGO R, RODRÍGUEZ-ROSALES M D J. ROJAS-MONTES J C, FUENTES-ACEITUNO J C, MARTÍNEZ-GÓMEZ V J. A kinetic-mechanistic study of cyanide degradation which can be contained in mining tailings dams using a divided electrolytic cell [J]. Minerals Engineering, 2022, 188: 107833.

[4] RAO S M, VENKATARAMA REDDY B V. Characterization of Kolar gold field mine tailings for cyanide and acid drainage [J]. Geotechnical & Geological Engineering, 2006, 24(6): 1545−1559.

[5] HAN Wen-wen, YANG Hong-ying, TONG Lin-lin. Cyanide removal for ultrafine gold cyanide residues by chemical oxidation methods [J]. Transactions of Nonferrous Metals Society of China, 2022, 32(12): 4129−4138.

[6] GUO Xu-yi, QIN Hong, TIAN Qing-hua, ZHANG Lei. The efficacy of a new iodination roasting technology to recover gold and silver from refractory gold tailing [J]. Journal of Cleaner Production, 2020, 261: 121147.

[7] KIVENTERÄ J, LANCELLOTTI I, CATAURO M, POGGETTO F D, LEONELLI C, ILLIKAINEN M. Alkali activation as new option for gold mine tailings inertization [J]. Journal of Cleaner Production, 2018, 187: 76−84.

[8] WANG Zhi-ming, WANG Qing, ZHAO Wei, XIA Chuan-bo, TIAN Xing-lei, JIANG Yun, ZHOU Xin, CHEN Guo-dong, WANG Li, CHEN Ming-gui. Influence of carlin-type gold mine tailings addition on the synthesis temperature, alkali-resistant performance, and hydration mechanism of Portland cement [J]. Construction and Building Materials, 2022, 359: 129458.

[9] WEI Zuo-an, ZHAO Jun-kang, WANG Wen-song, YANG Yong-hao, ZHUANG Sun-ning, LU Ting, HOU Zhen-kun. Utilizing gold mine tailings to produce sintered bricks [J]. Construction and Building Materials, 2021, 282: 122655.

[10] KIM Y, KIM M, SOHN J, PARK H. Applicability of gold tailings, waste limestone, red mud, and ferronickel slag for producing glass fibers [J]. Journal of Cleaner Production, 2018, 203: 957−965.

[11] HOSSEINI S M, VAKILCHAP F, BANIASADI M, MOUSAVI S M, KHODADADI D A, FARNAUD S. Green recovery of cerium and strontium from gold mine tailings using an adapted acidophilic bacterium in one-step bioleaching approach [J]. Journal of the Taiwan Institute of Chemical Engineers, 2022, 138: 104482.

[12] LIN Yue, HU Xian-zhi, ZI Fu-ting, CHEN Shu-liang, CHEN Yun-long, YANG Peng, ZHANG Yan, LI Xin-rong. Accelerating gold extraction from refractory gold tailings via NH_4HF_2 pre-treatment [J]. Journal of Molecular Liquids, 2023, 371: 121061.

[13] SNYDERS C A, AKDOGAN G, BRADSHAW S M, VAN VREDEN J H, SMITH R. The development of a caustic pre-leaching step for the recovery of Au from a refractory ore tailings heap [J]. Minerals Engineering, 2018, 121: 23−30.

[14] ZHANG Lei, JIANG Tao, GUO Xue-yi, TIAN Qing-hua, ZHONG Shui-ping, DONG Li, QIN Hong, LIU Zou-wei, MAKUZA B. Sustainable processing of gold cyanide tailings: Reduction roasting, mechanical activation, non-cyanide leaching, and magnetic separation [J]. Hydrometallurgy, 2023, 217: 106028.

[15] LIU Peng-fei, WANG Jun-jie, YU Da-wei, GUO Xue-yi, TIAN Qing-hun. Comprehensive reclamation of valuable metals from Au-bearing cyanide residue by chlorination roasting–carbothermic reduction–magnetic separation: recovery of iron [J]. Journal of Sustainable Metallurgy, 2021, 7(4): 1748−1761.

[16] LI Hao-yu, PENG Jin-hui, LONG Hai-lin, LI Shi-wei, ZHANG Li-bo. Cleaner process: Efficacy of chlorine in the recycling of gold from gold-containing tailings [J]. Journal of Cleaner Production, 2021, 287: 125066.

[17] QIN Hong, GUO Xue-yi, TIAN Qing-hua, ZHANG Lei. Pyrite enhanced chlorination roasting and its efficacy in gold and silver recovery from gold tailing [J]. Separation and Purification Technology, 2020, 250: 117168.

[18] FU Ping-feng, LI Zhen-yu, FENG Jie, BIAN Zhen-zhong. Recovery of gold and iron from cyanide tailings with a combined direct reduction roasting and leaching process [J]. Metals, 2018, 8(7): 561.

[19] GE Jian-hua, XIAO Yu-hua, KUANG Jun-er, LIU Xue-ming. Research progress of chlorination roasting of heavy metals in solid waste [J]. Surfaces and Interfaces, 2022, 29: 101744.

[20] IWASAKI I, PRASAD M S. Processing techniques for difficult-to-treat ores by combining chemical metallurgy and mineral processing [J]. Mineral Processing and Extractive Metallurgy Review, 1989, 4(3/4): 241−276.

[21] GUO Xue-yi, ZHANG Chun-xi, TIAN Qing-hua, YU Da-wei. Liquid metals dealloying as a general approach for the selective extraction of metals and the fabrication of nanoporous metals: A review [J]. Materials Today Communications, 2021, 26: 102007.

[22] SANTOS-MUNGUÍA P C, NAVA-ALONSO F, RODRÍGUEZ-CHÁVEZ V M, ALONSO-GONZÁLEZ O. Hidden gold in fire assay of gold telluride ores [J]. Minerals Engineering, 2019, 141: 105844.

[23] TIAN Qing-hua, GAN Xiang-dong, YU Da-wei, CUI Fu-hui, GUO Xue-yi. One-step and selective extraction of nickel from nickel-based superalloy by molten zinc [J]. Transactions of Nonferrous Metals Society of China, 2021, 31(6): 1828−1841.

[24] DING Yun-ji, ZHENG Huan-dong, ZHANG Shen-gen, LIU Bo, WU Bo-yu, JIAN Zhu-ming. Highly efficient recovery of platinum, palladium, and rhodium from spent automotive catalysts via iron melting collection [J]. Resources, Conservation and Recycling, 2020, 155: 104644.

[25] FORNALCZYK A, SATERNUS M. Removal of platinum group metals from the used auto catalytic converter [J]. Metalurgija, 2009, 48: 133−136.

[26] PENG Z W, LI Z Z, LIN X L, TANG H M, YE L, MA Y T, RAO M J, ZHANG Y B, LI G H, JIANG T. Pyrometallurgical recovery of platinum group metals from spent catalysts [J]. JOM, 2017, 69(9): 1553−1562.

[27] DONG Hai-gang, ZHAO Jia-chun, CHEN Jia-lin, WU Yue-dong, LI Bo-jie. Recovery of platinum group metals from spent catalysts: A review [J]. International Journal of Mineral Processing, 2015, 145: 108−113.

[28] ALCOCK C B, ITKIN V P, HORRIGAN M K. Vapour pressure equations for the metallic elements: 298−2500 K [J]. Canadian Metallurgical Quarterly, 1984, 23(3): 309−313.

[29] LIU Chuan, SUN Shu-chen, TU Gan-feng, XIAO Fa-xin. Co-treatment of spent automotive catalyst and cyanide tailing via vitrification and smelting-collection process for platinum group metals recovery [J]. Journal of Environmental Chemical Engineering, 2021, 9(5): 105823.

[30] LIU Ya, SONG Qing-ming, ZHANG Lin-gen, XU Zhen-ming. Novel approach of in-situ nickel capture technology to recycle silver and palladium from waste nickel-rich multilayer ceramic capacitors [J]. Journal of Cleaner Production, 2021, 290: 125650.

[31] CHEN Jing. Discussion on the micro-mechanism of precious metals trapped in pyro-metallurgical processes by base metals and matte phase [J]. Engineering Science, 2007, 9(5): 11−16.

[32] ZHOU Yan, LIU Jian-xing, CHENG Gong-jin, XUE Xiang-xin, YANG He. Carbothermal reduction followed by sulfuric acid leaching of Bayan Obo tailings for selective concentration of iron and rare earth metals [J]. Separation and Purification Technology, 2021, 271: 118742.

[33] KONG Ling-xue, BAI Jin, LI Wen, WEN Xiao-dong, LIU Xing-chen, LI Xiao-ming, BAI Zong-qing, GUO Zhen-xing, LI Huai-zhu. The internal and external factor on coal ash slag viscosity at high temperatures, Part 2: Effect of residual carbon on slag viscosity [J]. Fuel, 2015, 158: 976−982.

[34] XIAO Wen-bing, YAO Shin-wen, ZHOU Shi-wen, WEI Yong-gang, LI Bo, WANG Hua. Evolution of the structure and viscosity of copper slag during metallization-reduction [J]. Journal of Alloys and Compounds, 2022, 903: 163751.

[35] CHEN Zi-wei, WANG Hao, SUN Yong-qi, LIU Li-li, WANG Xi-dong. Insight into the relationship between viscosity and structure of $CaO-SiO_2-MgO-Al_2O_3$ molten slags [J]. Metallurgical and Materials Transactions B, 2019, 50(6): 2930−2941.

[36] KIM G H, SOHN I. Effects of alkali metal cations and fluoride anions on viscosity and structure of $CaO-SiO_2-Al_2O_3$ system [J]. Journal of Materials Research and Technology, 2022, 20: 2335−2347.

[37] CHENG Xiang-li, ZHAO Kai, QI Yuan-hong, SHI Xue-feng, ZHEN Chang-liang. Direct reduction experiment on iron-bearing waste slag [J]. Journal of Iron and Steel Research, International, 2013, 20(3): 24−35.

[38] KU Jian-gang, ZHANG Lin, FU Weng, WANG Shu-bin, YIN Wan-zhong, CHEN Hui-huang. Mechanistic study on calcium ion diffusion into fayalite: A step toward sustainable management of copper slag [J]. Journal of Hazardous Materials, 2021, 410: 124630.

[39] QAFOKU O, ILTON E S, BOWDEN M E, KOVARIK L, ZHANG X, KUKKADAPU R K, ENGELHARD M H, THOMPSON C J, SCHAEF H T, MCGRAIL B P, ROSSO K M, LORING J S. Synthesis of nanometer-sized fayalite and magnesium−iron(II) mixture olivines [J]. Journal of Colloid and Interface Science, 2018, 515: 129−138.

[40] SINEVA S, SHISHIN D, SHEVCHENKO M, HAYES P C, JAK E. Experimental study and thermodynamic modeling of distribution of elements among slag, matte and metal in the Cu−Fe−O−S−Si−(Zn)−(Al,Ca,Mg) system for copper slag cleaning applications [J]. Journal of Materials Research and Technology, 2023, 23: 5280−5300.

[41] SHISHIN D, HIDAYAT T, FALLAH-MEHRJARDI A, HAYES P C, DECTEROV S A, JAK E. Integrated experimental and thermodynamic modeling study of the effects of Al_2O_3, CaO, and MgO on slag–matte equilibria in the Cu−Fe−O−S−Si−(Al,Ca,Mg) system [J]. Journal of Phase Equilibria and Diffusion, 2019, 40(4): 445−461.

[42] YANNOPOULOS J C. Control of copper losses in reverberatory slags: A literature review [J]. Canadian Metallurgical Quarterly, 1971, 10(4): 291−307.

[43] HIDAYAT T, SHISHIN D, DECTEROV S A, JAK E. Critical assessment and thermodynamic modeling of the Cu−Fe−O−Si system [J]. Calphad, 2017, 58: 101−114.

[44] CHEN M, AVARMAA K, TASKINEN P, MICHALLIK R, JOKILAAKSO A. An experimental study on the phase equilibria of FeO_x-saturated iron silicate slags and metallic copper alloys at 1200−1300 °C [J]. Calphad, 2022, 77: 102418.

[45] HIDAYAT T, SHISHIN D, DECTEROV S A, JAK E. Experimental study and thermodynamic re-optimization of the $FeO-Fe_2O_3-SiO_2$ system [J]. Journal of Phase Equilibria and Diffusion, 2017, 38(4): 477−492.

[46] HAN Y S, SWINBOURNE D R, PARK J H. Thermodynamics of gold dissolution behavior in $CaO-SiO_2-Al_2O_3-MgO$ sat slag system [J]. Metallurgical and Materials Transactions B, 2015, 46: 2249−2457.

[47] HE Mei-le, CHEN Min, WANG Nan, LI Chuan-fu.

Sedimentation behavior of liquid iron droplets during smelting reduction of converter slag by considering the coalescence of droplets [J]. ISIJ International, 2019, 59(6): 973−980.

[48] ZHENG Huan-dong, DING Yun-ji, WEN Quan, ZHAO Shi-zhen, HE Xue-feng, ZHANG Shen-gen, DONG Chao-fang. Slag design and iron capture mechanism for recovering low-grade Pt, Pd, and Rh from leaching residue of spent auto-exhaust catalysts [J]. Science of the Total Environment, 2022, 802: 149830.

采用还原熔炼法回收氰化尾渣中的多金属元素

李嵩灏，焦 芬，李 琛，顾丝雨，刘世阳，魏 鑫

中南大学 资源加工与生物工程学院，长沙 410083

摘　要：提出了一种处理氰化尾渣的方法。还原熔炼使氰化尾渣中的银、铅和锌在高温下挥发，而金和铜与还原态铁结合形成金属相，实现多金属元素的共同回收。实验结果表明，最佳工艺条件为焦粉用量 7.5% (质量分数)、碱度 1.0、熔炼温度 1450 ℃以及熔炼时间 60 min。此条件下超过 99%的金、77%的铜和 94%的铁进入生铁，同时银的挥发率超过 90%，铅和锌基本完全挥发。副产物熔炼渣的主要成分为钙镁黄长石，浸出毒性低于国家标准，属于一般固废。此外，以铁对铜的捕集过程为例，分析铁的捕获机理，并将其分为熔炼还原、迁移捕集和凝聚沉积 3 个阶段。

关键词：氰化尾渣；金尾矿；还原熔炼；有价元素回收

(Edited by Wei-ping CHEN)